Supporting Information:

Iridium Complexes of the Conformationally Rigid IBioxMe$_4$ Ligand: Hydride Complexes and Dehydrogenation of Cyclooctene

Simone A. Hauser,[a] Ralf Tonner[b] and Adrian B. Chaplin[a,*]

[a] *Department of Chemistry, University of Warwick, Gibbet Hill Road, Coventry CV4 7AL, UK.*
E-mail: a.b.chaplin@warwick.ac.uk

[b] *Fachbereich Chemie, Philipps-Universität Marburg, Hans-Meerwein-Straße 4, D-35032 Marburg, Germany.*

Contents

1. Selected NMR spectra **S2**

2. Additional computational details **S9**

1. Selected NMR spectra

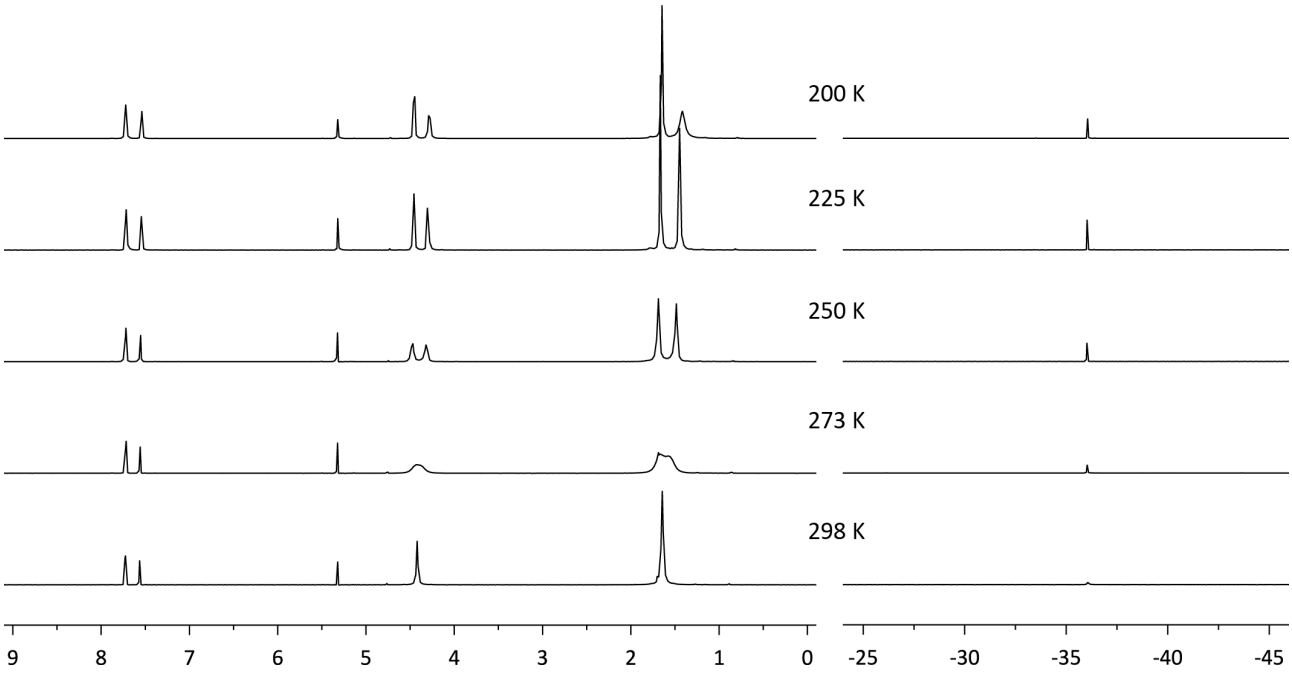

Figure S1: ^{1}H NMR spectra of **3** (CD_2Cl_2, 500 MHz).

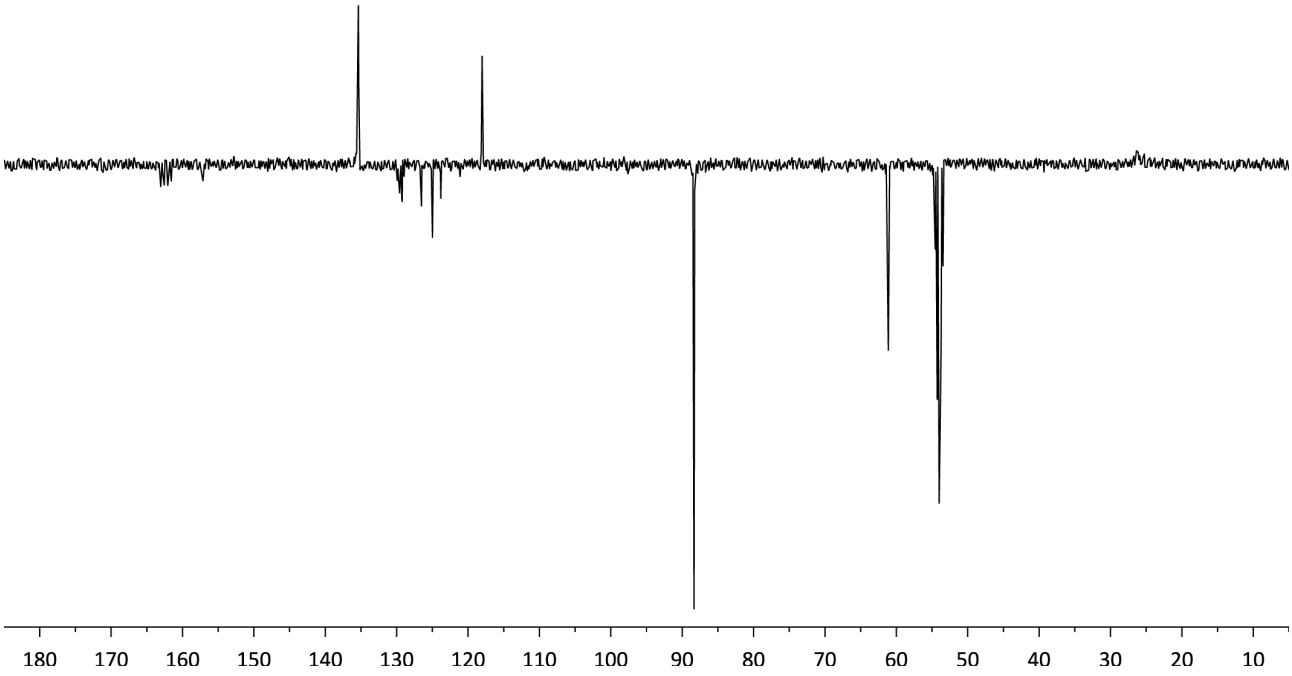

Figure S2: $^{13}C\{^{1}H\}$ PENDANT NMR spectrum of **3** (CD_2Cl_2, 101 MHz).

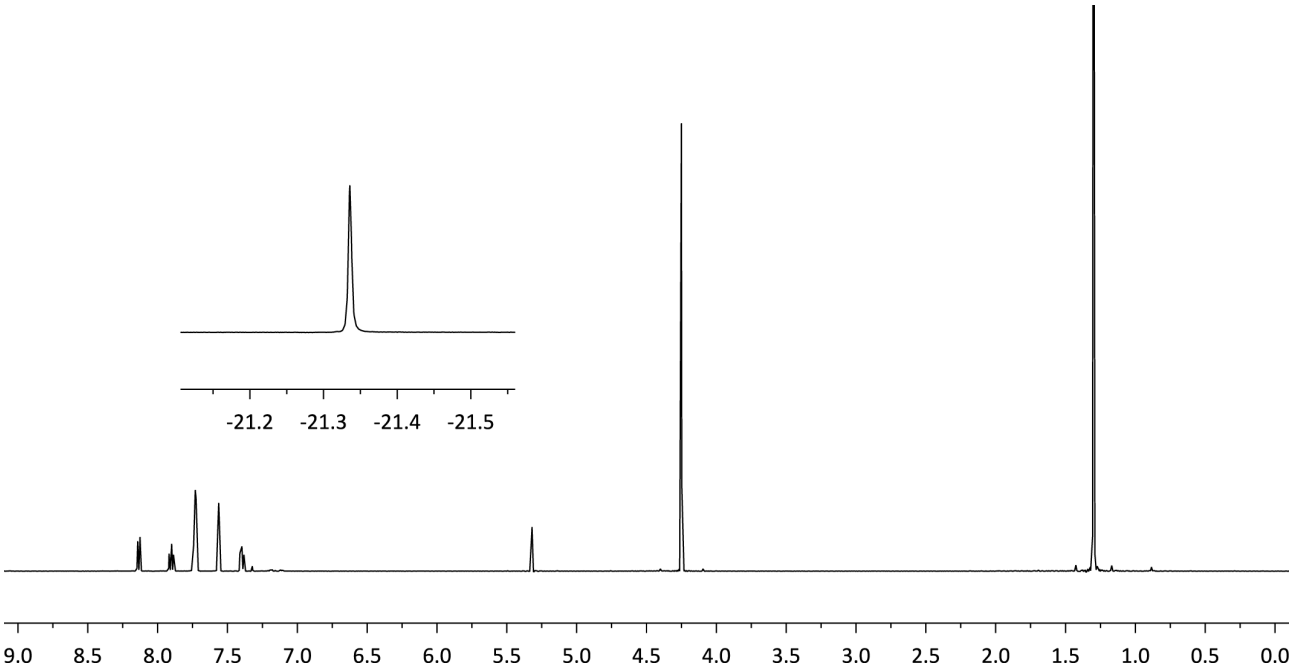

Figure S3: ^{1}H NMR spectrum of **4** (CD_2Cl_2, 500 MHz, hydride region not to scale).

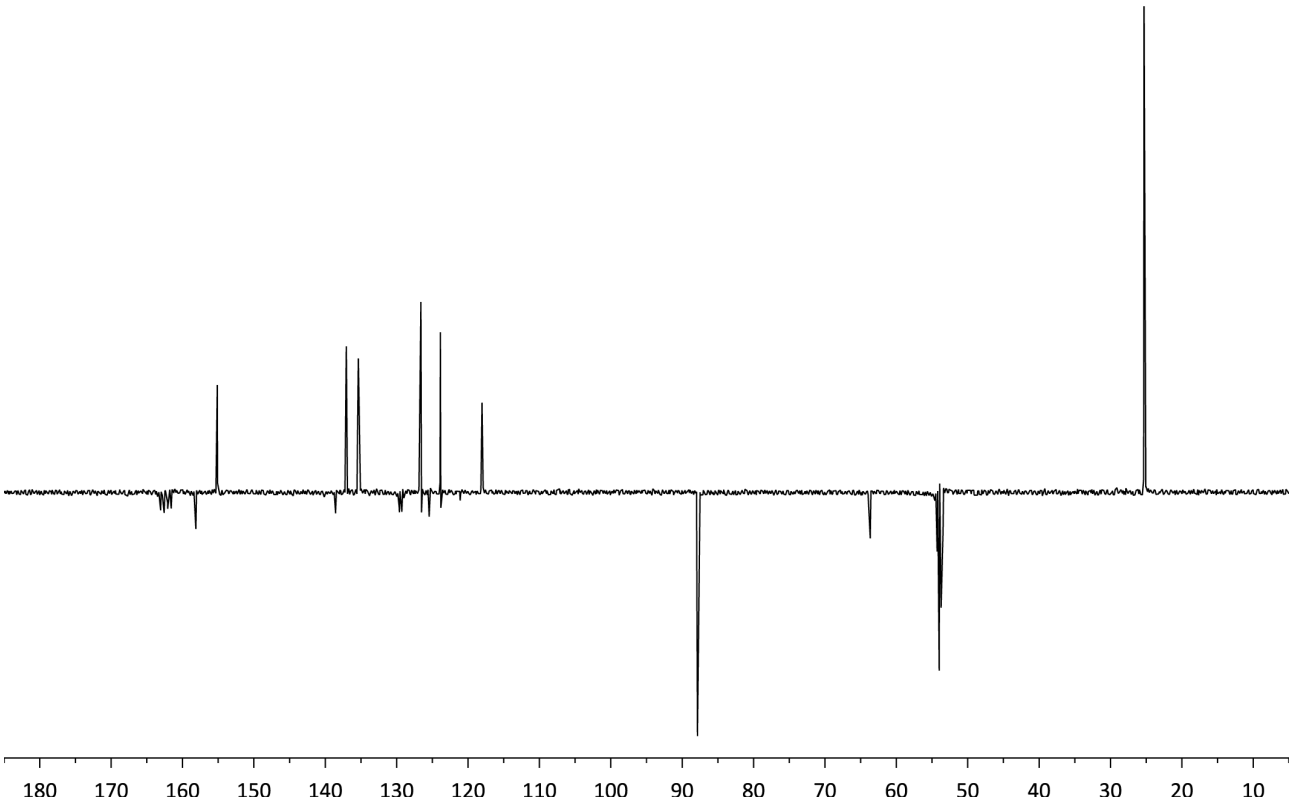

Figure S4: $^{13}C\{^{1}H\}$ PENDANT NMR spectrum of **4** (CD_2Cl_2, 101 MHz).

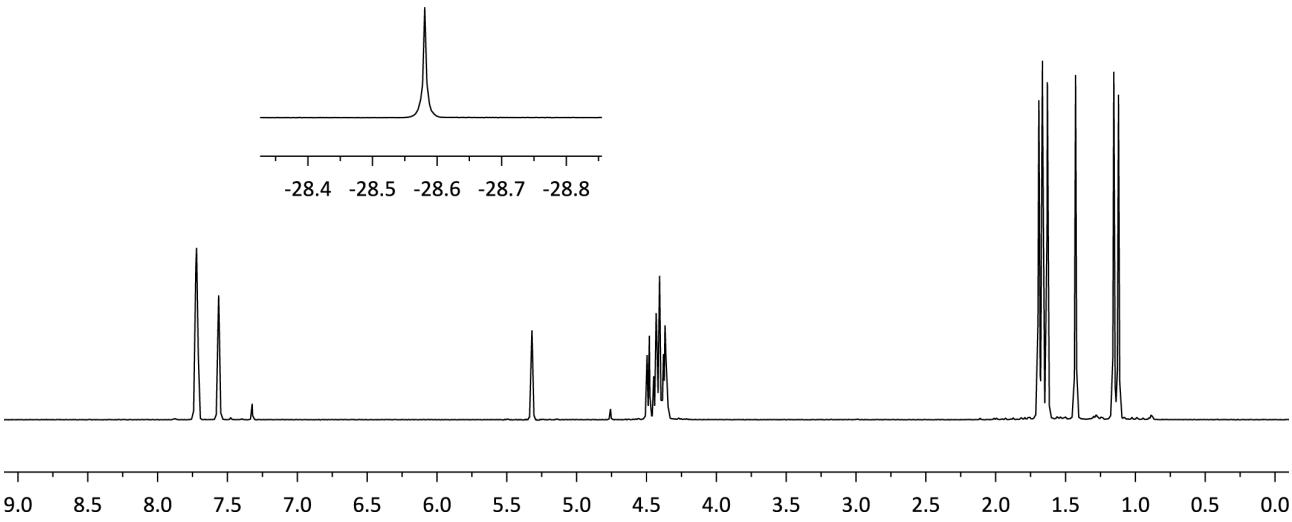

Figure S5: ^{1}H NMR spectrum of **5** (CD_2Cl_2, 500 MHz, hydride region not to scale).

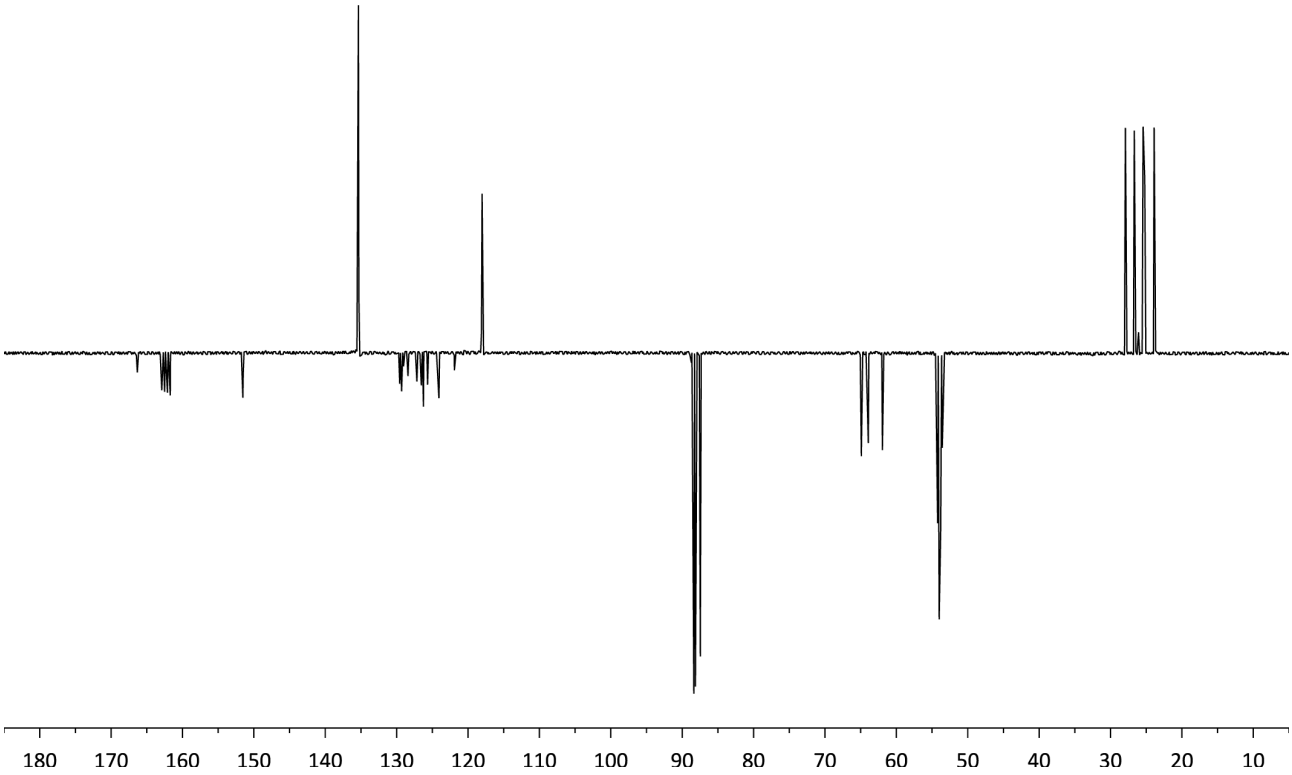

Figure S6: $^{13}C\{^{1}H\}$ APT NMR spectrum of **5** (CD_2Cl_2, 126 MHz).

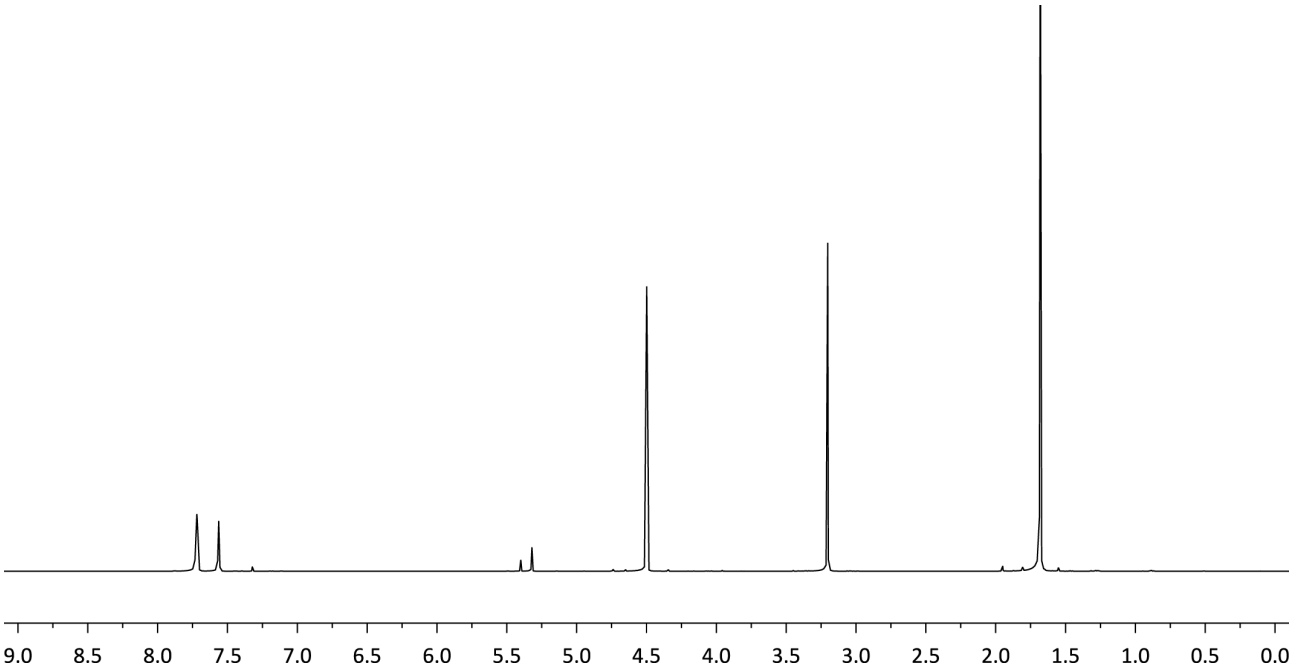

Figure S7: ^{1}H NMR spectrum of **6** (CD_2Cl_2, 500 MHz).

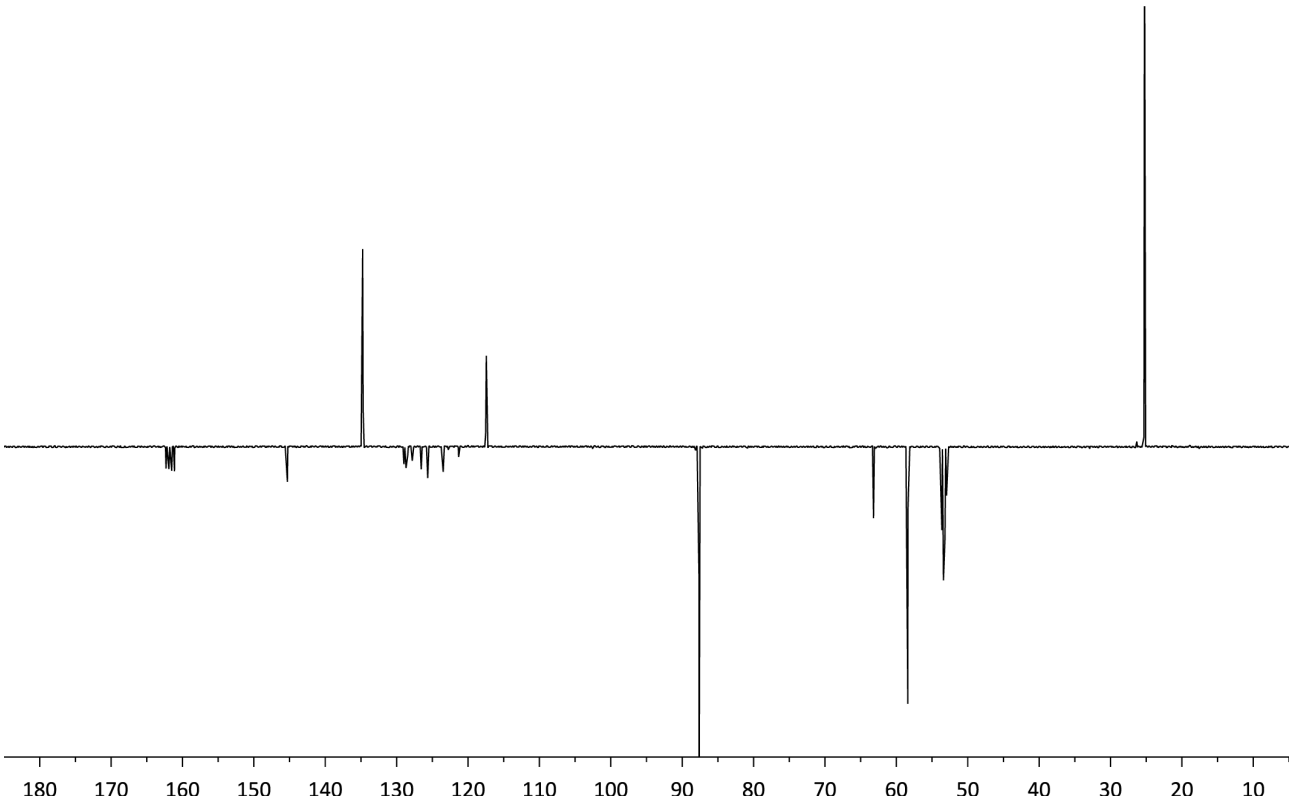

Figure S8: $^{13}C\{^{1}H\}$ APT NMR spectrum of **6** (CD_2Cl_2, 126 MHz).

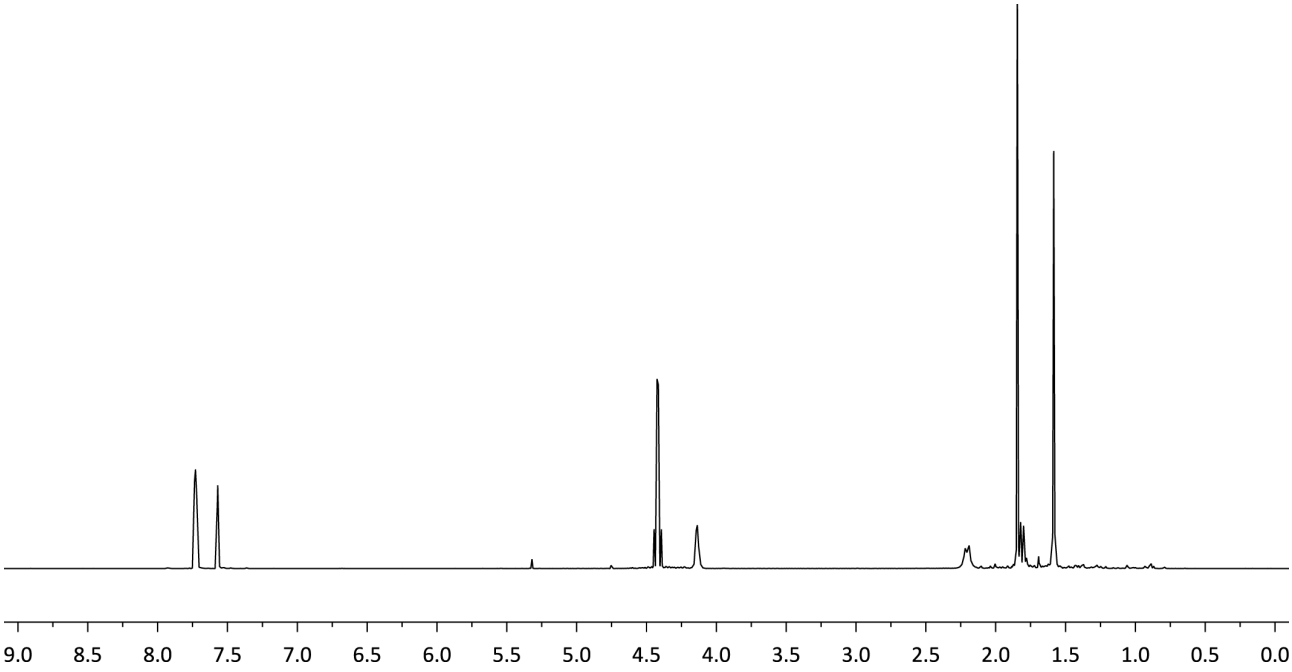

Figure S9: ^{1}H NMR spectrum of **7** (CD_2Cl_2, 400 MHz).

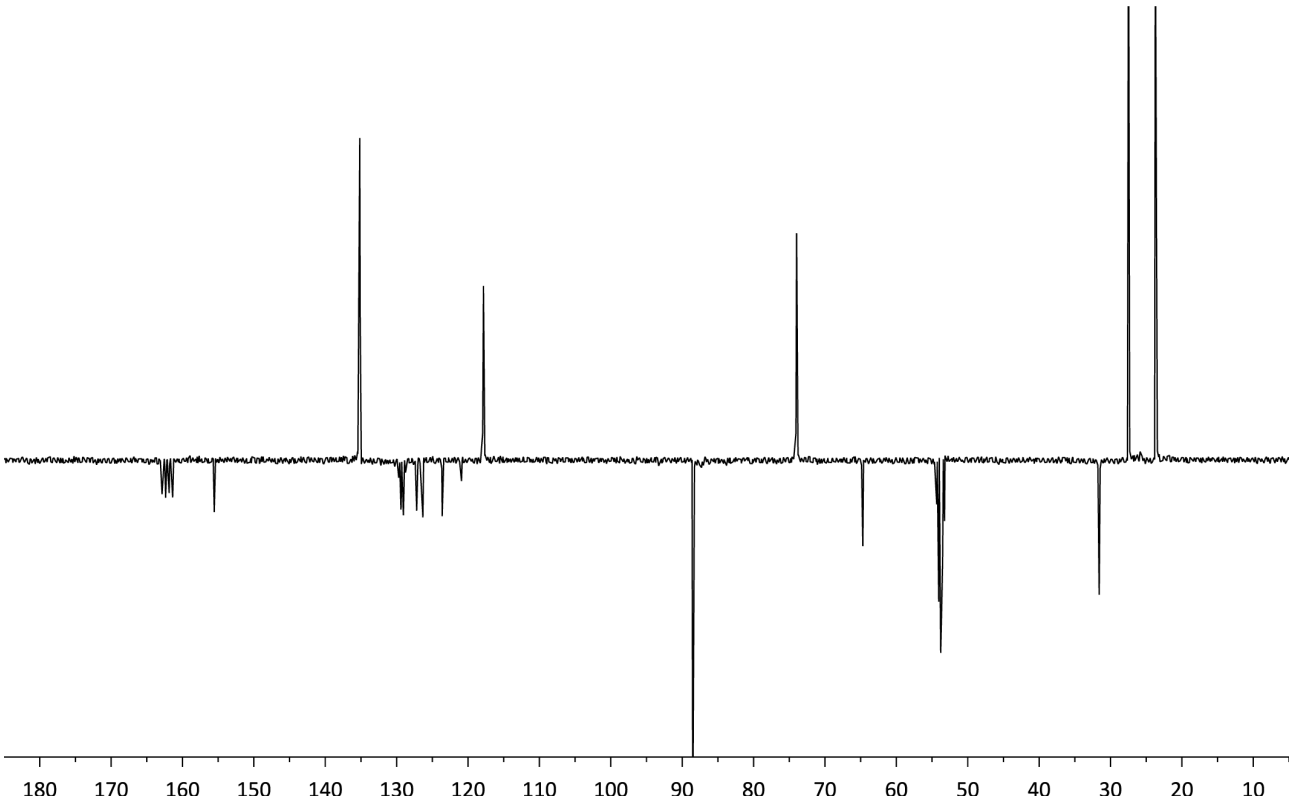

Figure S10: $^{13}C\{^{1}H\}$ PENDANT NMR spectrum of **7** (CD_2Cl_2, 101 MHz).

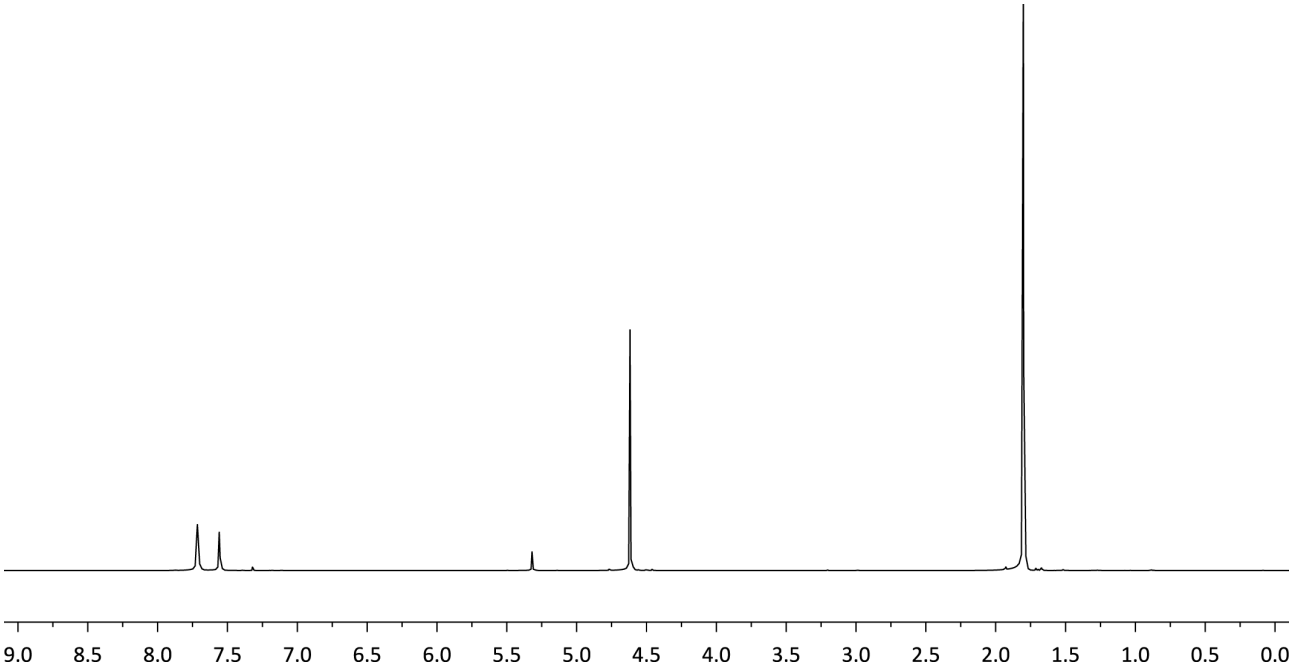

Figure S11: ^{1}H NMR spectrum of **8** (CD_2Cl_2, 500 MHz).

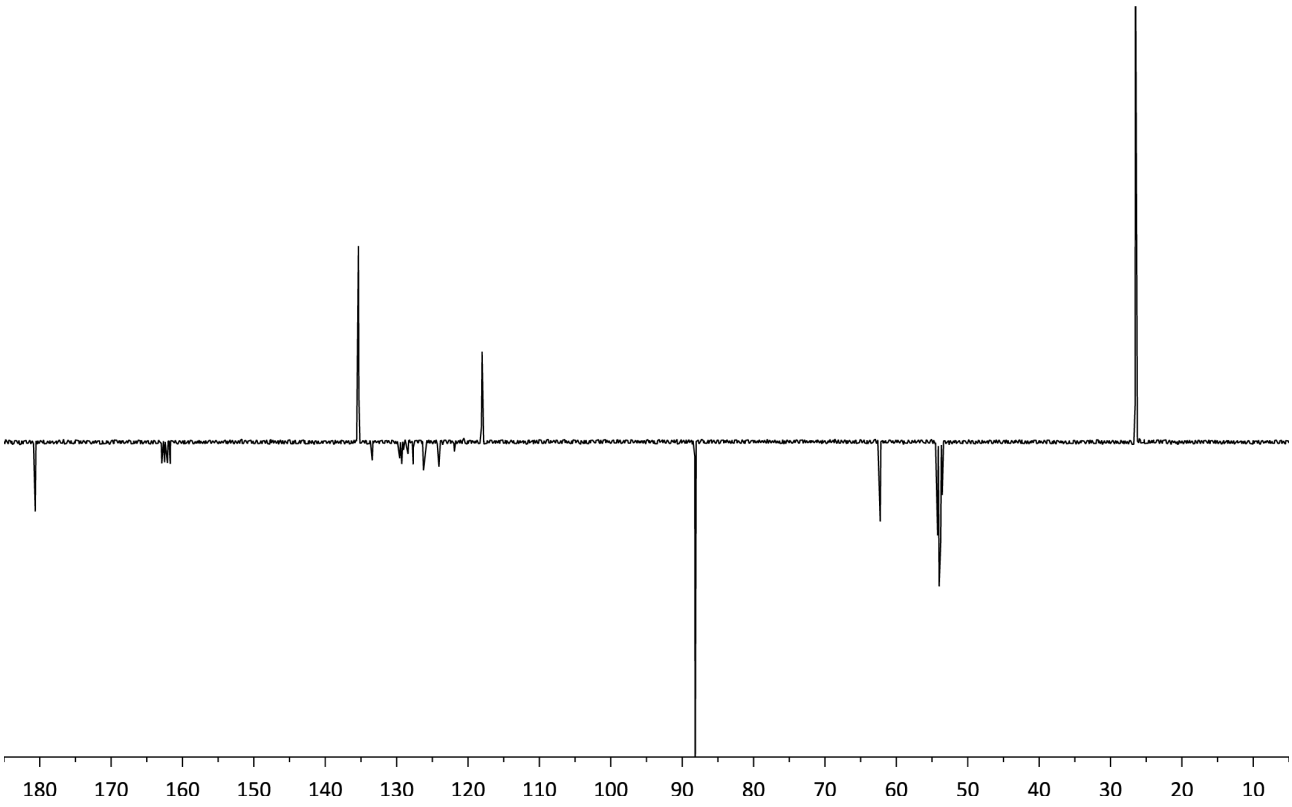

Figure S12: $^{13}C\{^{1}H\}$ APT NMR spectrum of **8** (CD_2Cl_2, 126 MHz).

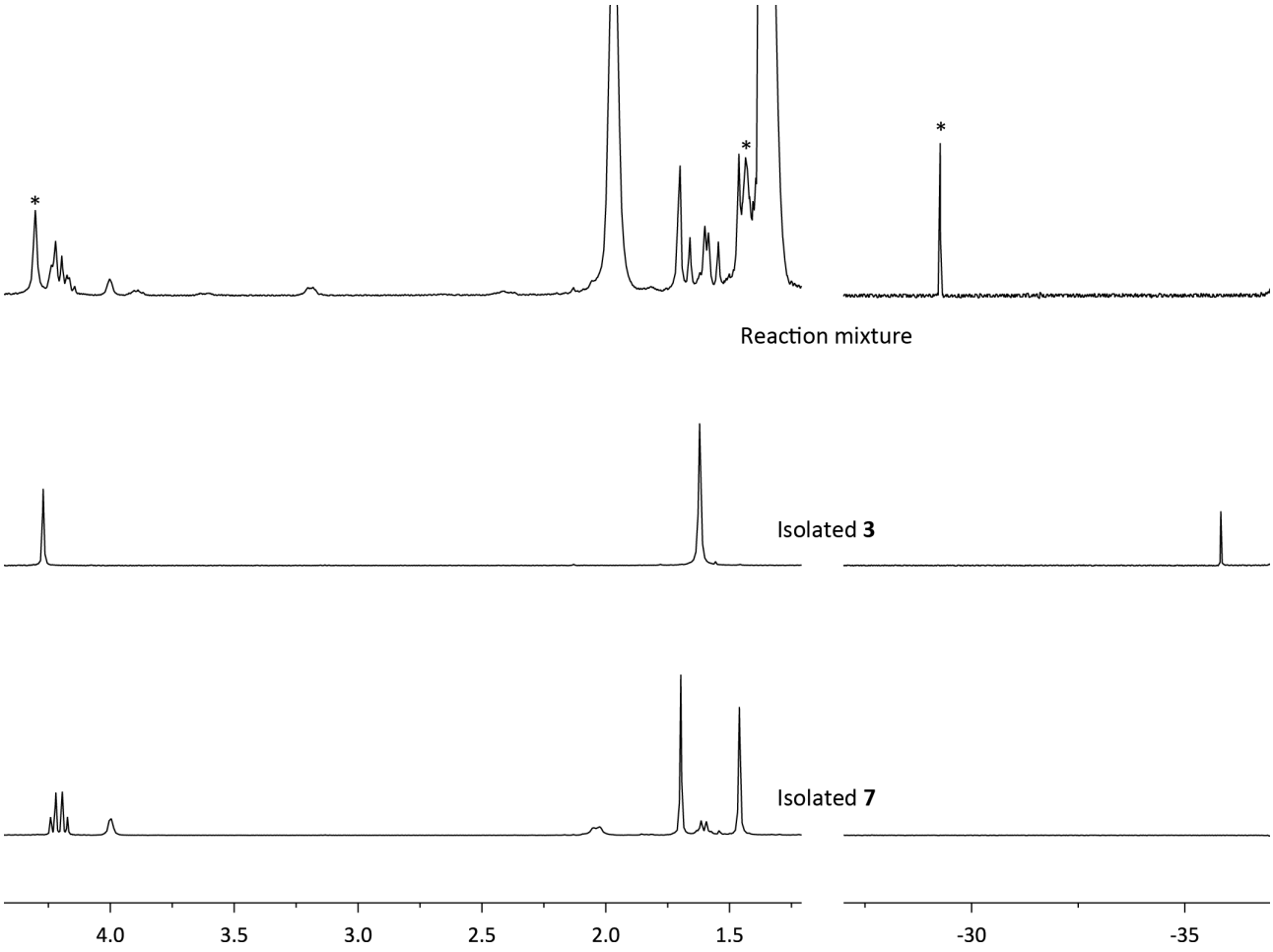

Figure S13: ^{1}H NMR spectrum recorded during the reaction of "**3** + Na[BAr^{F}_{4}]" and COE (ca. 6 h, 1,2-$C_6H_4F_2$, 400 MHz, hydride region at different scale). Spectra of isolated **3** and **7** included for comparison. * Assigned to major intermediate; integral ratio ~ 8 : 24 : 2 (high to low frequency resonances).

2. Additional computational details

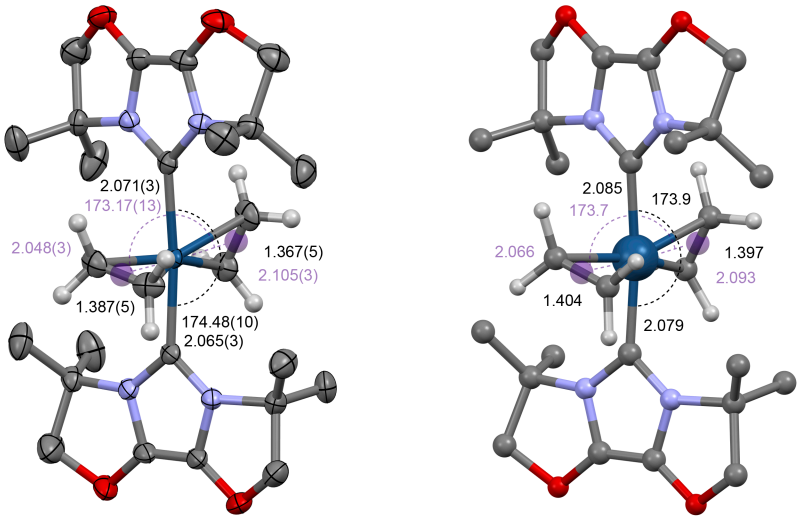

Figure S14. Solid-state (left, thermal ellipsoids drawn at the 50% probability level) and optimised (right, BP86-D3/def2-TZVPP) structures of the cationic component of **6** annotated with selected bond lengths (Å) and angles(º) – metrics associated with the alkene centroids in purple. Most hydrogen atoms omitted for clarity.

Table S1. Results from EDA-NOCV analysis (PBE-D3/TZ2P//BP86-D3/def2-TZVPP) for the fragmentation $[Ir(IBioxH_4)_2(C_2H_4)_2]^+$ → $[Ir(IBioxH_4)_2(C_2H_4)]^+ + C_2H_4$. Energies in units of kJ mol^{-1}. L1 = C_2H_4 perpendicular to C-M-C plane, L2 = C_2H_4 co-planar with C-M-C plane.

	6'				**6a'**		**6b'**	
	L1		L2					
ΔE_{int}	-261.5		-238.0		-231.3		-222.3	
ΔE_{disp}	-28.1		-23.9		-25.9		-25.2	
ΔE_{Pauli}	955.7		856.8		923.0		934.1	
ΔE_{elstat}	-671.0	(56%)	-624.8	(58%)	-652.0	(58%)	-648.6	(57%)
ΔE_{orb}	-518.2	(44%)	-446.1	(42%)	-476.4	(42%)	-482.7	(43%)
ΔE(M→L)	-236.7	(46%)	-224.7	(50%)	-270.8[a]	(57%)	-206.7[a]	(43%)
ΔE(L→M)	-227.5	(44%)	-175.1	(39%)	-138.8[a]	(29%)	-231.1[a]	(48%)
ΔE(*trans*-L(M)→L)[b]	-27.8	(5%)	-20.4	(5%)	-19.5	(4%)	0.0	
ΔE_{resid}	-26.2	(5%)	-25.9	(6%)	-47.3	(10%)	-45.0	(9%)
ΔE_{prep} (L)	45.4		35.3		47.3		41.2	
ΔE_{prep} (M)	48.7		35.1		23.9		93.4	
ΔE_{prep}	94.1		70.3		71.1		134.6	
ΔE_{bond} (=-D_e)	-167.4		-167.6		-160.2		-87.7	

[a] contributions mix and cannot unambiguously be separated

[b] The deformation densities (e.g. $\Delta\rho_3$ in Figure S15) show charge-flow from the C_2H_4 ligand bound *trans* to the dissociated ligand. Intra-fragment polarization (charge flow from *trans*-C_2H_4 to iridium atom) can also be found in $\Delta\rho_3$.

$\Delta\rho_1$
M→L1

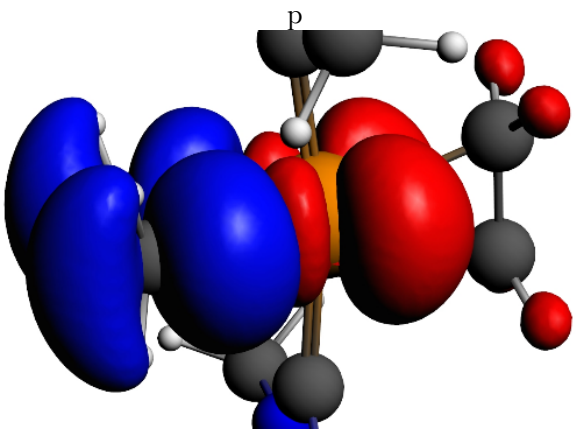

ΔE_1 = -236.7 v_1 = ±0.793

$\Delta\rho_2$
L1→M

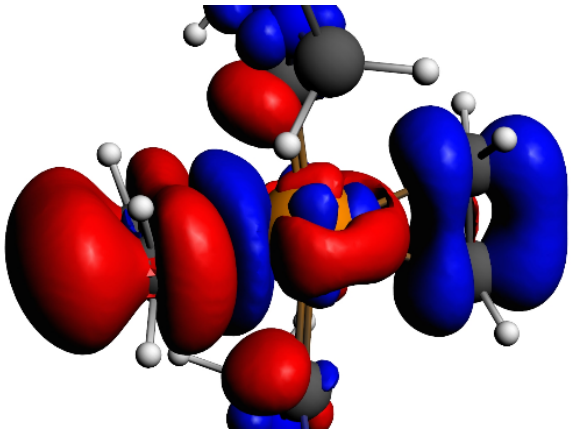

ΔE_2 = -217.6 v_2 = ±0.768

$\Delta\rho_3$
L2(M)→L1

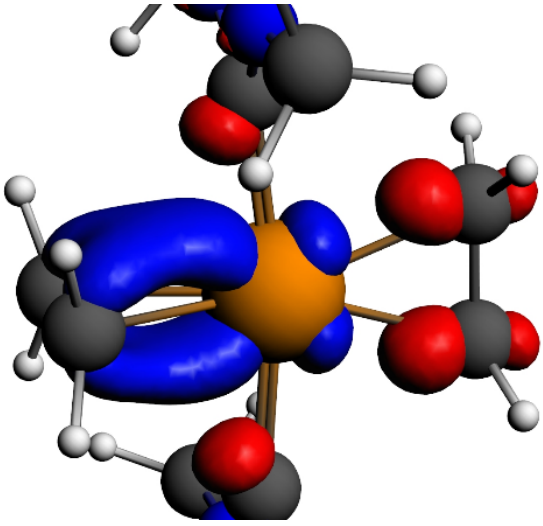

ΔE_3 = -27.8 v_3 = ±0.163

$\Delta\rho_4$
L1→M

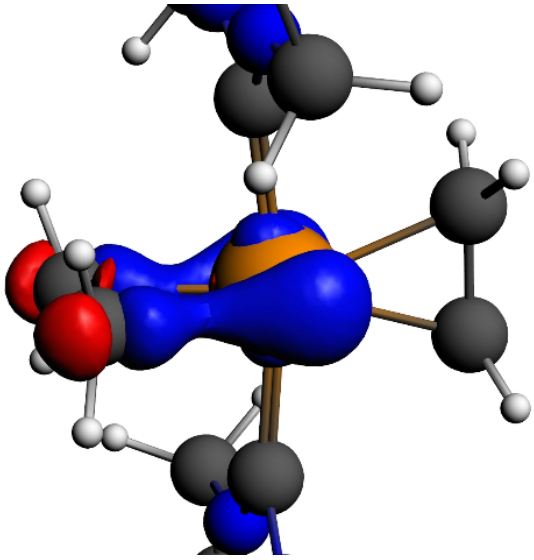

ΔE_4 = -9.9 v_4 = ±0.156

Figure S15: Selected deformation densities for L1 + M-L2 for **6'**.